

The settling of nonspherical particles in a cellular flow field

R. Mallier and M. Maxey

Division of Applied Mathematics, Brown University, Providence, Rhode Island 02912

(Received 19 June 1990; accepted 7 February 1991)

The motion of rigid spheroidal particles settling under gravity in a spatially periodic, cellular flow field has been studied. The particles are sufficiently small that their motion relative to the surrounding fluid satisfies the conditions for local Stokes flow, and the force and couple on the particle are linearly related to the local flow conditions. The motion of each particle depends on the orientation of its symmetry axis, which turns in response to the local vorticity and rate of strain. For spherical shapes the cellular flow field generally can hold particles in permanent suspension, as they move in simple closed paths, over a significant portion of each cell. By comparison, for nonspherical shapes this suspension is greatly reduced, though not eliminated. The individual particles undergo a tumbling motion as they settle which, at large enough aspect ratios, is found to be chaotic.

I. INTRODUCTION

A common question in the study of particles settling under gravity in a nonuniform flow is whether or not the particles can be held in suspension by the flow, and if not what effect does the flow have on the average settling velocity. As an example, Stommel¹ has studied the gravitational settling of small, spherical particles in a convection cell flow. The flow is incompressible, steady and two dimensional, and may be specified by a streamfunction ψ as

$$\psi = U_0 L \sin(x_1/L) \sin(x_2/L). \quad (1)$$

The net force on each particle is approximately zero; as the particle responds rapidly to the local flow conditions, and at each instant the velocity of the particle is the sum of the local fluid velocity and the terminal fall velocity due to gravity. Stommel showed over a significant portion of each cell particles may be held in permanent suspension by the flow, moving in simple closed paths, provided that the terminal fall speed was less than the maximum updraft velocity in the flow, U_0 . More recent work^{2,3} has shown that if the effects of particle inertia are included, this permanent suspension is no longer possible and that all particles settle out. Indeed the average settling velocity is generally greater than the terminal fall speed in the absence of any flow.

Of significance is the assumption that the particles are spherical in shape. In many situations of practical interest where solid particles are being transported by a flow, the particles may be distinctly nonspherical. Examples of this include the formation and growth of crystals in a liquid melt, ice crystal growth in atmospheric clouds,⁴ and crystal formation in a cooling body of magma.⁵ The size to which these particles grow and how the flow will ultimately develop will depend on how long the particles are suspended by the flow.

In these contexts the departures from a spherical shape are often more significant than other influences such as particle inertia. Liquid melts and magmas are characteris-

tically very viscous flows, and the densities of the particles in the flow and of the liquid phase are comparable. The fluid forces on the particles, even for particles of several millimeters in size, are accurately described by Stokes flow with negligible fluid inertia and by the same token negligible particle inertia. Very small aerosol particles may also be significantly nonspherical yet exhibit little effects of particle inertia. Unlike solids in a liquid phase, the density of an aerosol particle is much greater than that of the surrounding air and particle inertia becomes significant more quickly for increasing particle size even though fluid forces may be still well described by Stokes flow results. In atmospheric clouds ice crystals smaller than 20 μm in size will not typically show effects of particle inertia, yet will be distinctly nonspherical and for diameters greater than 5 μm unaffected by Brownian motion. In this study we focus on the changes in particle motion that arise for nonspherical particles settling under gravity and exclude other modifying factors.

An aim of this paper is to investigate the motion of nonspherical particles in the cellular flow (1), to determine the extent to which particle suspension by the flow still occurs, and to evaluate the average settling velocity. A second aim of this paper is to obtain more general insights into the behavior of nonspherical particles settling in spatially varying flows and possible insights as to their motion in turbulent flows. Only in a loose, qualitative sense is the periodic cellular flow field representative of turbulent eddies of small-scale mixing, but previous studies^{6,7} have shown its value in studies of dispersion. The advantage is that this flow is amenable to analysis and it is inexpensive to compute particle trajectories. Our own experience^{2,8} is that the results can alert one to features arising in a turbulent flow that would be missed by a straightforward statistical analysis.

An early study of the motion of nonspherical particles in a fluid was the paper by Jeffery.⁹ He considered an ellipsoidal particle that was neutrally buoyant and was

placed in a uniform shear flow. The forces and moments acting on the small particle were determined by the Stokes flow produced by the particle moving relative to the flow. In this example the center of the particle moved with the fluid but the particle turned in response to the vorticity and rate of strain. Jeffery showed that the particle rotates in a regular periodic motion. Brenner,^{10,11} and Dill and Brenner,¹² in a series of papers have analyzed the dispersion of nonspherical particles settling under gravity while subject to the effects of Brownian motion. In this context the fluid is at rest but the particles rotate under agitation by Brownian motion and as they do the direction of the terminal fall velocity changes. The particles do not settle vertically but at various random angles to the vertical, which leads to a lateral dispersion. Cho *et al.*,¹³ Kagermann and Koehler,¹⁴ and Krushkal and Gallily,¹⁵ amongst others, have investigated the settling and dispersion of nonspherical particles in turbulence. These studies have focused on deriving evolution equations for the statistical properties.

In this paper we consider the combined effects of a spheroidal particle turning in response to the local velocity gradient and the changes in gravitational settling velocity that occur as the particle turns. In Sec. II we summarize the equations governing the motion of a small spheroidal particle and give the specific form they take for the cellular flow field. In subsequent sections we examine the retention of particles in the flow, the tumbling motion of settling particles, and the onset of chaotic motion that is found to occur at larger aspect ratios.

II. EQUATIONS OF PARTICLE MOTION

The simplest nonspherical particle shape to consider is the spheroid, or ellipsoid of revolution, which is specified by the two lengths of its principal diameters. These will be denoted as $2a$, the diameter along the axis of symmetry, and $2b$, the diameter orthogonal to the axis of symmetry. Ellipsoidal particles belong to the more general class of orthotropic particles,^{16,17} namely those with three mutually orthogonal planes of reflectional symmetry. In this paper we restrict our attention to the motion of spheroidal particles of uniform composition, though for the moment we will give the equations of motion for a more general orthotropic particle. The motion of any rigid particle is specified by the velocity \mathbf{V} of its center of mass and the angular velocity $\boldsymbol{\Omega}$ about this point. We will denote the instantaneous position of its center of mass by $\mathbf{X}(t)$.

A small, isolated rigid particle when it is introduced into a flow field $\mathbf{u}(\mathbf{x},t)$ produces a local disturbance flow $\mathbf{v}(\mathbf{x},t)$ such that the sum of the two forms the resultant modified flow. The boundary conditions governing the disturbance flow are that $|\mathbf{v}|$ tends to zero far from the particle and that for points on the surface of the particle, the no-slip condition applies. The particle is supposed to be sufficiently small that any velocity gradients of the undisturbed flow may be accurately regarded as being locally uniform. For points \mathbf{x} on the surface of the moving particle the no-slip condition is

$$\mathbf{v} = \mathbf{V} - \mathbf{u}(\mathbf{X}(t),t) + \boldsymbol{\Omega} \times (\mathbf{x} - \mathbf{X}) - (\mathbf{x} - \mathbf{X}) \cdot \nabla \mathbf{u}, \quad (2)$$

or in terms of the local rate of strain tensor \mathbf{E} and the local vorticity $\boldsymbol{\omega}$ of the undisturbed flow,

$$\mathbf{v} = \mathbf{V} - \mathbf{u}(\mathbf{X}(t),t) + (\boldsymbol{\Omega} - \frac{1}{2}\boldsymbol{\omega}) \times (\mathbf{x} - \mathbf{X}) - (\mathbf{x} - \mathbf{X}) \cdot \mathbf{E}, \quad (3)$$

where \mathbf{E} and $\boldsymbol{\omega}$ are evaluated at $\mathbf{X}(t)$. If the scale W_0 is taken to be representative of the slip velocity $[\mathbf{V} - \mathbf{u}(\mathbf{X}(t),t)]$ and β is representative of the local fluid velocity gradients, then the disturbance flow \mathbf{v} will be a Stokes flow provided

$$aW_0/\nu \ll 1, \quad a^2\beta/\nu \ll 1, \quad (4)$$

where we further suppose that a is representative of the size of the particle and the angular velocity $\boldsymbol{\Omega}$ is comparable to β in magnitude. The linearity of the equations for Stokes flow and the form of the boundary condition (3) ensure that the resultant fluid force \mathbf{F} on the particle and the torque \mathbf{G} are linearly related to the slip velocity, relative rate of rotation ($\boldsymbol{\Omega} - \frac{1}{2}\boldsymbol{\omega}$) and rate of strain by tensors that depend only on the size and shape of the particle, and by the fluid viscosity μ .

The reflectional symmetries of an orthotropic particle simplify the nature of these Faxen relations¹⁶ to give

$$\mathbf{F}_i = \mu K_{ij} [u_j(\mathbf{X}(t),t) - V_j(t)], \quad (5)$$

$$\mathbf{G}_i = \mu R_{ij} (\frac{1}{2}\omega_j - \Omega_j) + \mu D_{ijk} E_{jk}, \quad (6)$$

while the Reciprocal Theorem¹⁶ for Stokes flow ensures that both R and K are symmetric, proper tensors. The pseudotensor D_{ijk} is symmetric in the components for j and k . Further, the reflectional symmetries imply that the principal axes of K and R both coincide with the symmetry axes of the particle. When referred to these principal axes the relations (5) and (6) take a particularly simple form and the tensor components D_{ijk} only take nonzero values if the three indices are distinct.

Consistent with the assumption of low Reynolds numbers (4) we will further neglect the influence of particle inertia for sufficiently small particles. The motion of the particle is then specified by the condition that there is no net force or torque acting on the particle. Because of gravity there will be a force $m_p \mathbf{g}$ on a particle of mass m_p , suitably modified to take account of buoyancy if this is relevant, where \mathbf{g} is the gravitational acceleration vector. The condition of no net force implies that $(\mathbf{F} + m_p \mathbf{g})$ vanishes. When referred to the principal (symmetry) axes this condition from (5), leads to the result for the particle velocity

$$V_i = u_i(\mathbf{X}(t),t) + w_i, \quad (7)$$

where w_i are the three components of the terminal fall velocity ($m_p g_1 / \mu K_{11}$, $m_p g_2 / \mu K_{22}$, $m_p g_3 / \mu K_{33}$) for a particle settling in still fluid. Similarly, when referred to principal axes the condition of no net torque, which for a particle of uniform composition is that \mathbf{G} vanishes, gives the angular velocity of the particle

$$\Omega_1 = \frac{1}{2}\omega_1(\mathbf{X}(t),t) + D_1 E_{23}, \quad (8a)$$

$$\Omega_2 = \frac{1}{2}\omega_2(\mathbf{X}(t),t) + D_2 E_{13}, \quad (8b)$$

$$\Omega_3 = \frac{1}{2} \omega_3(X(t), t) + D_3 E_{12}, \quad (8c)$$

from (6) with

$$D_1 = 2D_{123}/R_{11} \quad (9)$$

and corresponding definitions for D_2 and D_3 .

We restrict attention now to the motion of axisymmetric particles. For these the specification of principal axes is simply determined from the unit vector \mathbf{m} , aligned with the axis of symmetry. This symmetry vector rotates with the body and

$$\frac{d\mathbf{m}}{dt} = \boldsymbol{\Omega} \times \mathbf{m}. \quad (10)$$

Principal components are determined by whether they are parallel or normal to \mathbf{m} . The two principal fall speeds W_1 and W_2 are defined, respectively, as the terminal fall speed for a particle settling parallel to the axis of symmetry \mathbf{m} or normal to it. Thus if $\hat{\mathbf{g}}$ denotes the unit vector in the direction of gravity the general form for the particle velocity (7) is

$$\mathbf{V}(t) = \frac{d\mathbf{X}}{dt} = \mathbf{u}(\mathbf{X}(t), t) + W_1(\hat{\mathbf{g}} \cdot \mathbf{m})\mathbf{m} + W_2[\hat{\mathbf{g}} - (\hat{\mathbf{g}} \cdot \mathbf{m})\mathbf{m}]. \quad (11)$$

Symmetry conditions^{16,18} for axisymmetric particles imply that $D_1 = 0$ and that $D_3 = -D_2$; we simply denote D_3 by D from here on. The angular velocity (8) of the particle is

$$\boldsymbol{\Omega}(t) = \frac{1}{2} \boldsymbol{\omega}(\mathbf{X}(t), t) + D\mathbf{m} \times (\mathbf{E} \cdot \mathbf{m}). \quad (12)$$

Equations (10)–(12) are sufficient together with the values of the parameters W_1 , W_2 , and D to determine the motion of any small axisymmetric, orthotropic particle in a nonuniform flow.

A. Spheroidal particles

Specific values for fall speeds W_1 and W_2 , and the parameter D can be given for spheroidal particles. Jeffery⁹ in his study of spheroidal particles in a uniform shear has evaluated the tensors used in (5) and (6) and additional results are given by Bretherton.¹⁸ The basic parameter to specify is the aspect ratio $\lambda = a/b$ for the spheroidal shape. In terms of this the ratio of W_1 to W_2 may be evaluated since W_1 and W_2 are, respectively, $m_p g / \mu K_{11}$ and $m_p g / \mu K_{22}$,

$$W_2/W_1 = \Lambda = K_{11}/K_{22}. \quad (13)$$

For a prolate spheroid, $\lambda > 1$ and with $\tau^2 = \lambda^2 - 1$,

$$\Lambda = \frac{1}{2} \frac{[(2\tau^2 - 1)\log(\lambda + \tau) + \lambda\tau]}{[(2\tau^2 + 1)\log(\lambda + \tau) - \lambda\tau]}. \quad (14)$$

For an oblate spheroid, $\lambda < 1$ and with $\tau^2 = 1 - \lambda^2$,

$$\Lambda = \frac{1}{2} \frac{[(2\tau^2 + 1)\tan^{-1}(\tau/\lambda) - \lambda\tau]}{[(2\tau^2 - 1)\tan^{-1}(\tau/\lambda) + \lambda\tau]}. \quad (15)$$

A spherical particle has aspect ratio one and the two principal fall speeds are equal, $\Lambda = 1$. Figure 1 shows the variation of Λ with aspect ratio λ , as Λ varies between 1.5 for

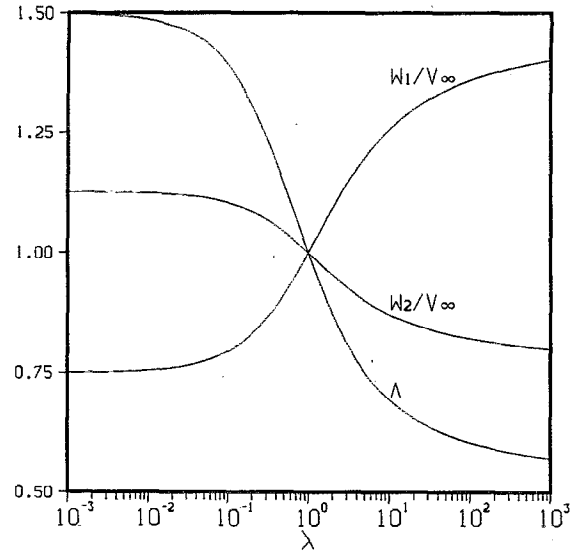


FIG. 1. Variation of the ratio of the principal settling velocities $\Lambda = W_2/W_1$ with the aspect ratio λ for a spheroidal particle. Also shown are the ratios of W_1 and W_2 to V_∞ .

disk-shaped particles, $\lambda = 0$, and 0.5 for cigar-shaped particles where λ becomes very large.

The value of the parameter D determines the degree to which the particle turns in response to the local rate of strain. This is given in terms of the aspect ratio λ by

$$D = (\lambda^2 - 1)/(\lambda^2 + 1), \quad (16)$$

and varies between the values of -1 for disk-shaped particles (oblate) to $+1$ for cigar-shaped particles (prolate). A particle will continue to rotate indefinitely in response to vorticity (12) but will turn with the rate of strain only until the axis of symmetry aligns with one of the principal axes of the rate of strain. In a pure straining flow and where \mathbf{E} takes a fixed value, then a prolate spheroid will turn until the axis of symmetry is aligned with the principal axis of greatest positive strain rate. There is an asymptotic preference for this alignment. Conversely, an oblate spheroid will tend to align with the symmetry axis parallel to the principal axis of largest negative strain rate.

Rather than specifying the value of W_1 and then inferring the value of W_2 from the value of the ratio Λ it is useful to define a spherically averaged fall speed. This would be the average fall speed of a particle with uniformly random orientation settling in still fluid. This spherically averaged fall speed V_∞ is

$$V_\infty = \frac{1}{3}(W_1 + 2W_2), \quad (17)$$

and in terms of this

$$W_1/V_\infty = 3/(2\Lambda + 1), \quad (18)$$

$$W_2/V_\infty = 3\Lambda/(2\Lambda + 1). \quad (19)$$

The value of V_∞ permits an easier comparison of the behavior of spherical and nonspherical particles. The variation of W_1/V_∞ and W_2/V_∞ with aspect ratio is also shown in Fig. 1.

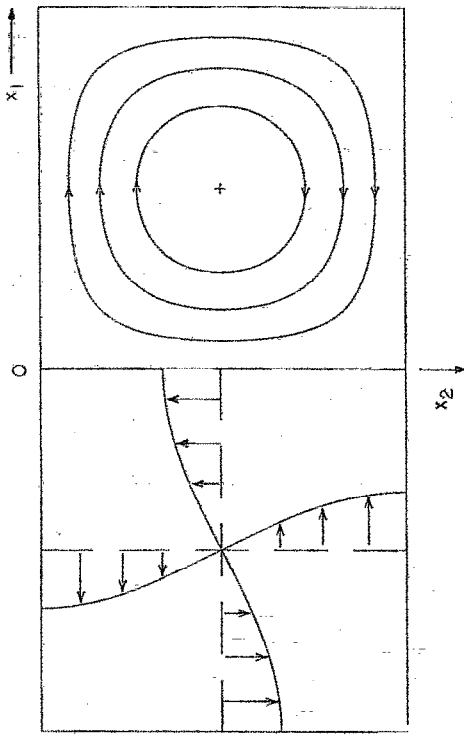


FIG. 2. Typical velocity profiles and streamline patterns for the cellular flow field in the horizontal region $-1 < x_1 < 1$. Stagnation points lie at the flow corners and the center of each cell.

B. Motion in a cellular flow

The preceding derivations have been fairly general and apply equally to many different flows. In this paper we consider the effects of the two-dimensional cellular flow given by the streamfunction ψ in (1). The scale U_0 for the maximum flow speed is set equal to one and the size of each cell is chosen so that $L=1/\pi$. The corresponding velocity field in fixed coordinates is

$$\mathbf{u} = (u_1, u_2, 0) = (\sin \pi x_1 \cos \pi x_2, -\cos \pi x_1 \sin \pi x_2, 0), \quad (20)$$

and the x_2 axis is aligned vertically downward parallel to $\hat{\mathbf{g}}$. Some typical velocity profiles and streamlines are shown in Fig. 2. The flow extends with periodic repetition in both the x_1 and x_2 directions, and is spatially uniform in x_3 . The maximum flow occurs on the cell boundaries, and there are stagnation points at the center of each cell and at the corners. The corresponding vorticity vector $\boldsymbol{\omega}$ has only one nonzero component, perpendicular to the plane of the flow, $\boldsymbol{\omega} = (0, 0, \omega)$, where

$$\omega = 2\pi \sin \pi x_1 \sin \pi x_2. \quad (21)$$

The rate of strain tensor has two nonzero components $E \equiv E_{11} = -E_{22}$ where

$$E = \pi \cos \pi x_1 \cos \pi x_2. \quad (22)$$

The equations of motion for a spheroidal particle [(10)–(12)] now take the form

$$V_1 = u_1 + (W_1 - W_2)m_1m_2, \quad (23a)$$

$$V_2 = u_2 + W_2 + (W_1 - W_2)m_2^2, \quad (23b)$$

$$V_3 = (W_1 - W_2)m_2m_3, \quad (23c)$$

combined with (20) and with (21) and (22)

$$\frac{dm_1}{dt} = -\frac{1}{2}\omega m_2 + DE m_1(m_3^2 + 2m_2^2), \quad (24a)$$

$$\frac{dm_2}{dt} = \frac{1}{2}\omega m_1 - DE m_2(m_3^2 + 2m_1^2), \quad (24b)$$

$$\frac{dm_3}{dt} = DE m_3(m_2^2 - m_1^2). \quad (24c)$$

The rate of rotation depends both on the particle orientation and local flow conditions, which change as the particle moves. The velocity and orientation of the particle are closely coupled and the system of equations (23) and (24) governing the particle motion have a complicated structure, much more so than for motion in a uniform shear.^{9,18}

To better understand the particle dynamics a restricted system will be considered, namely the symmetry axis will be constrained to lie in the (x_1, x_2) plane. A particle initially introduced and aligned in the plane, $m_3=0$, will remain aligned in the plane as indicated by (24c). This alignment condition may also give a better indication of what may occur in a general flow varying in all three spatial directions. The important feature introduced in studying nonspherical particles is the difference in the two principal fall speeds W_1 and W_2 . The effect of this difference is determined by the orientation components m_1 and m_2 . A particle with alignment out of the plane presents a lower projected aspect ratio onto the plane and so reduces the influence of this feature. Alternatively, we may note that $0 \leq m_1^2, m_2^2 \leq 1 - m_3^2$ and the maximum values of m_1 and m_2 are reduced if m_3 is nonzero. For these reasons we consider this restricted problem with the expectation, borne out by preliminary tests, that these results are typical of the general behavior.

Under this condition that m_3 vanishes, both V_3 and dm_3/dt remain zero and the equations of motions (23) and (24) can be expressed as

$$V_1 = \sin \pi X_1 \cos \pi X_2 + (W_1 - W_2) \sin \theta \cos \theta, \quad (25a)$$

$$V_2 = -\cos \pi X_1 \sin \pi X_2 + W_2 + (W_1 - W_2) \sin^2 \theta, \quad (25b)$$

$$\begin{aligned} \frac{d\theta}{dt} = & \pi \sin \pi X_1 \sin \pi X_2 \\ & - 2D\pi \cos \pi X_1 \cos \pi X_2 \sin \theta \cos \theta. \end{aligned} \quad (25c)$$

The orientation of the particle in the (x_1, x_2) plane is specified here by the angle θ , $m_1 = \cos \theta$ and $m_2 = \sin \theta$. This system of three coupled, nonlinear equations may be solved numerically. The results presented in the remaining sections were obtained by using standard predictor-corrector schemes¹⁹ or fourth-order Runge-Kutta methods.

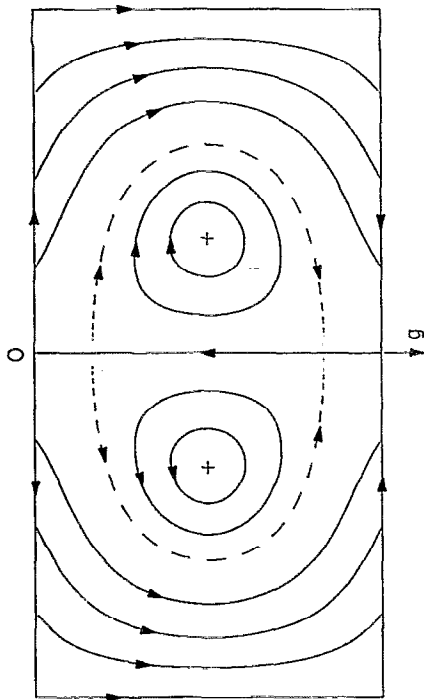


FIG. 3. Sample paths of spherical particles settling in the cellular flow field: $W=0.5$. The broken line denotes the boundary trajectory separating the trapping and settling regions; + denotes interior static equilibrium point.

III. PARTICLE SUSPENSION

The first aspect of the particle motion to be considered is whether or not spheroidal particles may be suspended by the flow. As noted earlier a spherical particle may be permanently suspended in certain regions of the cellular flow field and will follow a simple closed path. The motion of a spherical particle is conveniently given by a particle streamfunction ϕ obtained from (1),

$$\phi = \psi - V_{\infty} x_1 = (1/\pi) \sin(\pi x_1) \sin(\pi x_2) - V_{\infty} x_1, \quad (26)$$

with $V_1 = \partial\phi/\partial x_2$ and $V_2 = -\partial\phi/\partial x_1$, and since the terminal fall speeds W_1 and W_2 are equal these are also equal to V_{∞} from (17). Suspension is possible for $V_{\infty} < 1$. Sample particle trajectories for spherical particles, which illustrate these closed paths in the upflow region of the cell, are shown in Fig. 3. There is a bounding path emanating from the equilibrium points on the cell boundary corresponding to $\phi = 0$, outside of which the particles settle, swept downwards by the downflow in this other region of the cell. Disregarding the rotation of the sphere, as this is decoupled from the velocity of the particle, the spatial equilibrium points for a sphere are saddle points at

$$X_1 = 0, \quad X_2 = (1/\pi) \sin^{-1}(V_{\infty}), \quad (27a)$$

$$X_1 = 0, \quad X_2 = 1 - (1/\pi) \sin^{-1}(V_{\infty}), \quad (27b)$$

and a center at

$$X_1 = (1/\pi) \cos^{-1}(V_{\infty}), \quad x_2 = \frac{1}{2}. \quad (28)$$

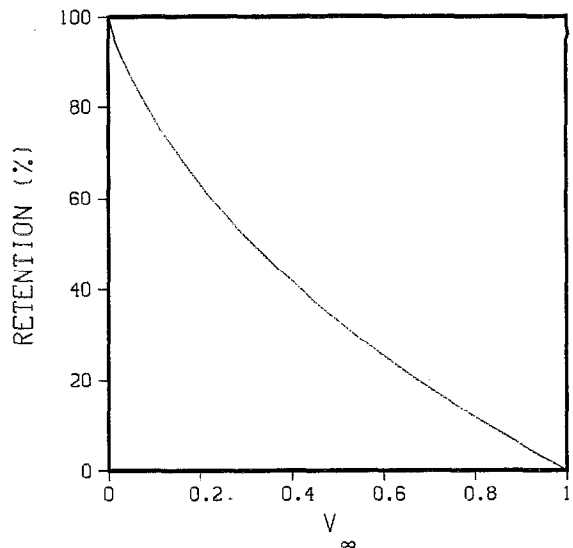


FIG. 4. Percentage of an initially uniform spatial distribution of spherical particles permanently suspended, as a function of Stokes settling velocity.

These are determined from (25) for the cell $0 < x_1 < 1$ and $0 < x_2 < 1$, and corresponding points exist for the other cells.

The extent of the particle suspension may be measured by the fraction of the area enclosed by the bounding trajectory compared to that of the cell as a whole. This is shown in Fig. 4. If particles were initially introduced into the flow with a uniform spatial distribution this area fraction would equal the fraction of the number of particles that would be suspended in the flow. Clearly no equilibrium points [(27) and (28)] exist if $V_{\infty} > 1$ and under these conditions all particles settle out.

In going to the motion of a spheroidal particle a number of changes occur. First, the particle orientation θ is no longer decoupled, and as the particle turns the velocity of the particle (25) will change. If the orientation is included, even for a sphere, the center (28) is no longer an equilibrium point since the particle would continue to rotate. The possible equilibrium points for the cells $-1 < x_1 < 1$ and $0 < x_2 < 1$ all lie on the cell boundary $X_1 = 0$, with

$$X_2 = (1/\pi) \sin^{-1}(W_2), \quad \theta = 0, \quad (29a)$$

$$X_2 = 1 - (1/\pi) \sin^{-1}(W_2), \quad \theta = 0, \quad (29b)$$

$$X_2 = (1/\pi) \sin^{-1}(W_1), \quad \theta = \pi/2, \quad (30a)$$

$$X_2 = 1 - (1/\pi) \sin^{-1}(W_1), \quad \theta = \pi/2. \quad (30b)$$

The values of W_1 and W_2 are equal for a sphere and the points (29) and (30) match the single pair of equilibrium points (27), except that for a sphere there is no restriction on the value of θ .

The distinction between suspension and settling of spheroidal particles is no longer clear-cut. The particle paths, even in what may be regarded as a region of particle suspension, are complex curves. This is illustrated by the sample trajectories shown in Fig. 5, computed for the time interval $t=0-50$ during which each particle remained

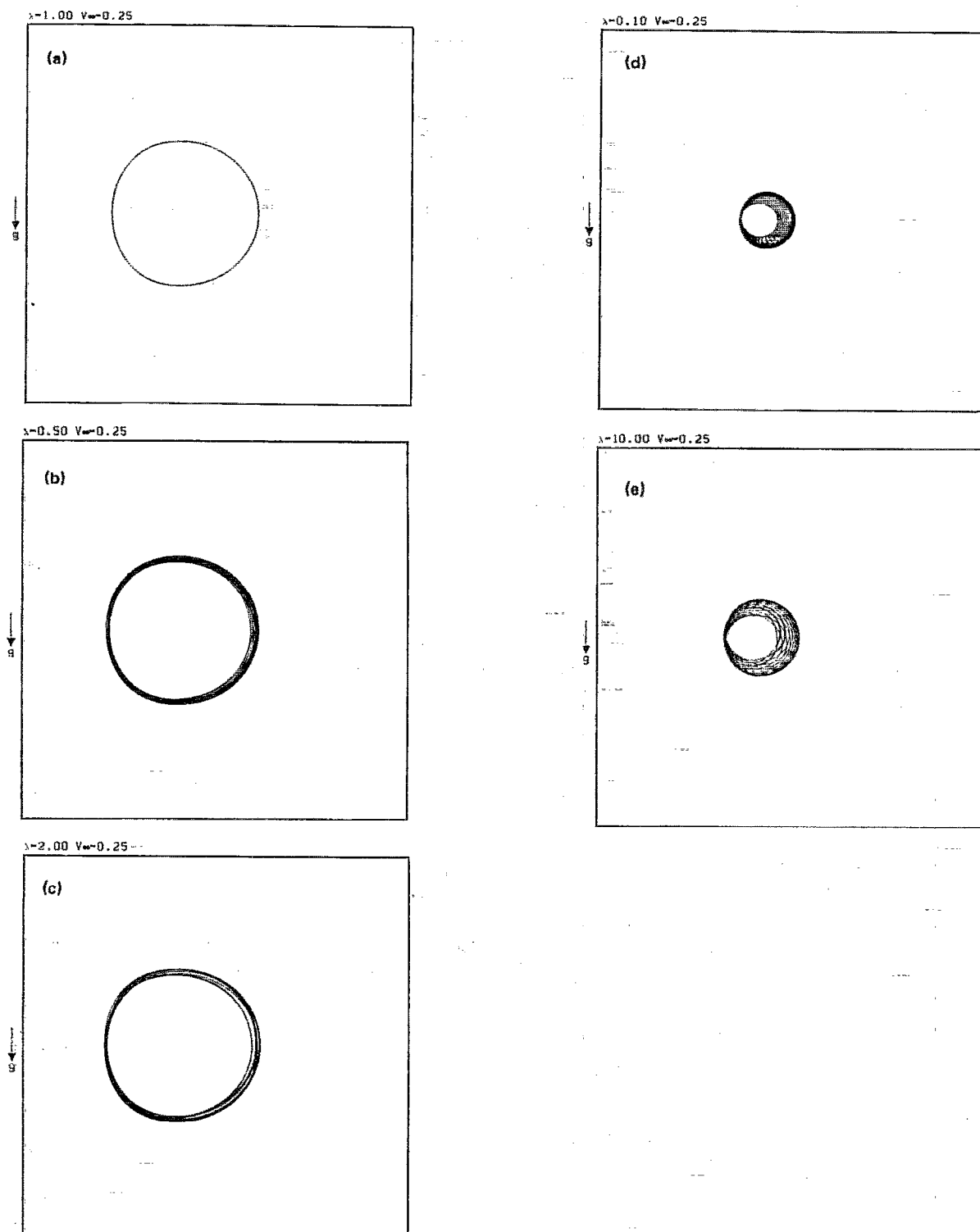


FIG. 5. Typical paths in the (x_1, x_2) plane of spheroidal particles suspended by the cellular flow field. All trajectories shown lie within the cell $0 < x_1, x_2 < 1$ and the spherically averaged settling velocity $V_w = 0.25$: (a) $\lambda = 1.0$, initial point $(X_1, X_2) = (0.6875, 0.4375)$; (b) $\lambda = 0.5$, initial point as in (a); (c) $\lambda = 2.0$, initial point as in (a); (d) $\lambda = 0.1$, initial point $(0.5625, 0.4375)$; (e) $\lambda = 10.0$, initial point as in (d).

within the initial cell. The sequence of Figs. 5(a)–5(c) is for a particle introduced at the same initial point but with different aspect ratios: $\lambda = 1$, a sphere; $\lambda = 0.5$, an oblate spheroid; and $\lambda = 2.0$, a prolate spheroid. These show the influence of the particle rotation on particle velocity. At higher aspect ratios, Figs. 5(d) and 5(e), suspension is still

possible for a different initial position, but the precession in the particle path is more pronounced. —

The extent of particle suspension was determined by releasing 500 particles at $t=0$ within the cell $0 < x_1 < 1$, $0 < x_2 < 1$. The particles were introduced with random, uniformly distributed initial positions and orientations and

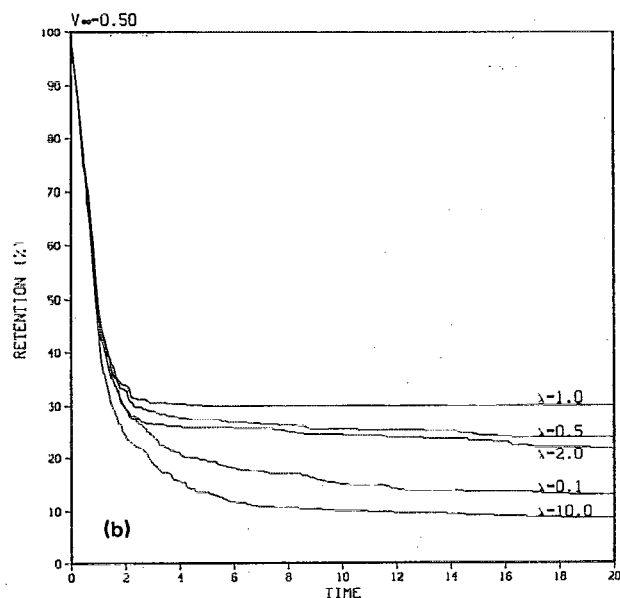
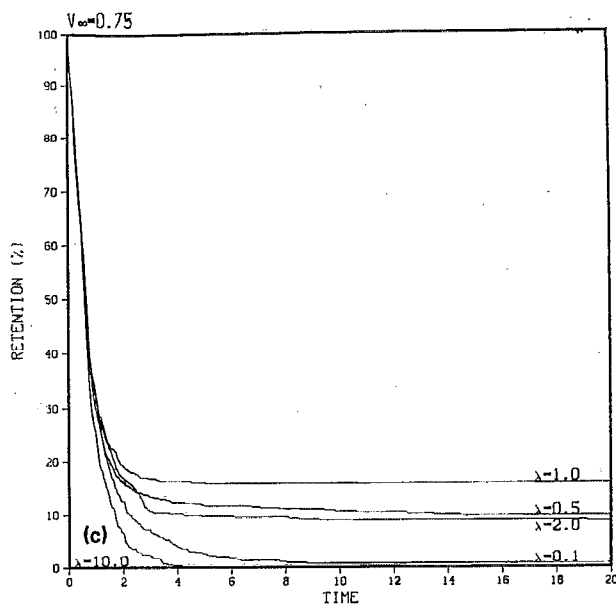
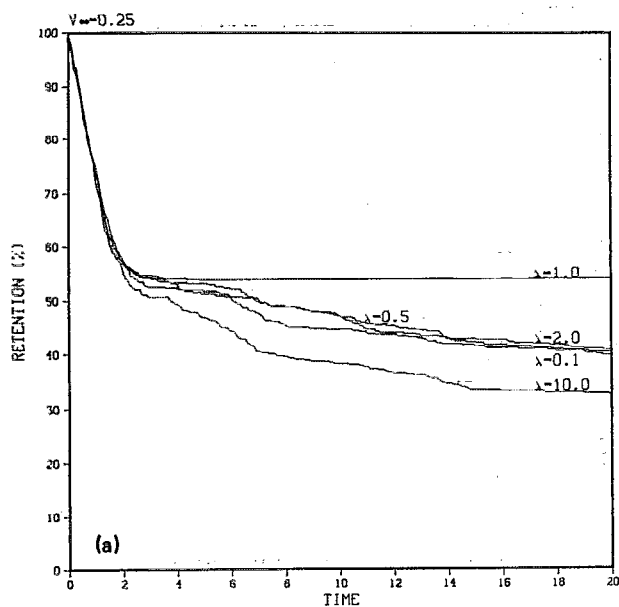


FIG. 6. Percentage of spheroidal particles retained as a function of time for the various aspect ratios λ indicated: (a) $V_\infty = 0.25$; (b) $V_\infty = 0.5$; (c) $V_\infty = 0.75$.

their motion recorded. Figure 6 shows the percentage of these particles at later times which are still retained in the initial cell and which have not crossed out of the cell. This has been calculated for different values of V_∞ and aspect ratios λ . Soon after the particles are introduced a large portion is swept out of the cell by the downflow region. This is much the same whether the particles are spherical or not. Subsequently, the number of spherical particles retained equilibrates to a steady value, as given in Fig. 3(b), while the number of nonspherical particles retained continues to slowly decrease at least for some time. Long-term suspension still appears to occur but is significantly reduced.

Another view of the extent to which long-term suspension occurs is presented in Fig. 7. Particles were introduced at $x_2 = \frac{1}{2}$ with different initial values of the horizontal coord-

inate x_1 in the range $0 < x_1 < 1$, and with different initial orientations θ between 0 and π . These were arranged on a uniform 50×50 grid. The motion of each particle was followed for up to $t = 50$ to determine whether or not the particle remained in the initial cell. The points shown in the diagrams record the initial values of those particles still suspended in the flow. Any spherical particle introduced in the interval $0 < x_1 < x_1^*$, where x_1^* solves

$$\sin(\pi x_1^*) / \pi x_1^* = V_\infty, \quad (31)$$

irrespective of initial orientation would be suspended. For $V_\infty = 0.5$, as in Fig. 7, the value of x_1^* is 0.603. The results indicate that for moderate aspect ratios, $\lambda = 2$ or 0.5 , particles remain suspended over a substantial range with only a slight dependence on orientation. At $V_\infty = 0.5$, 48% and

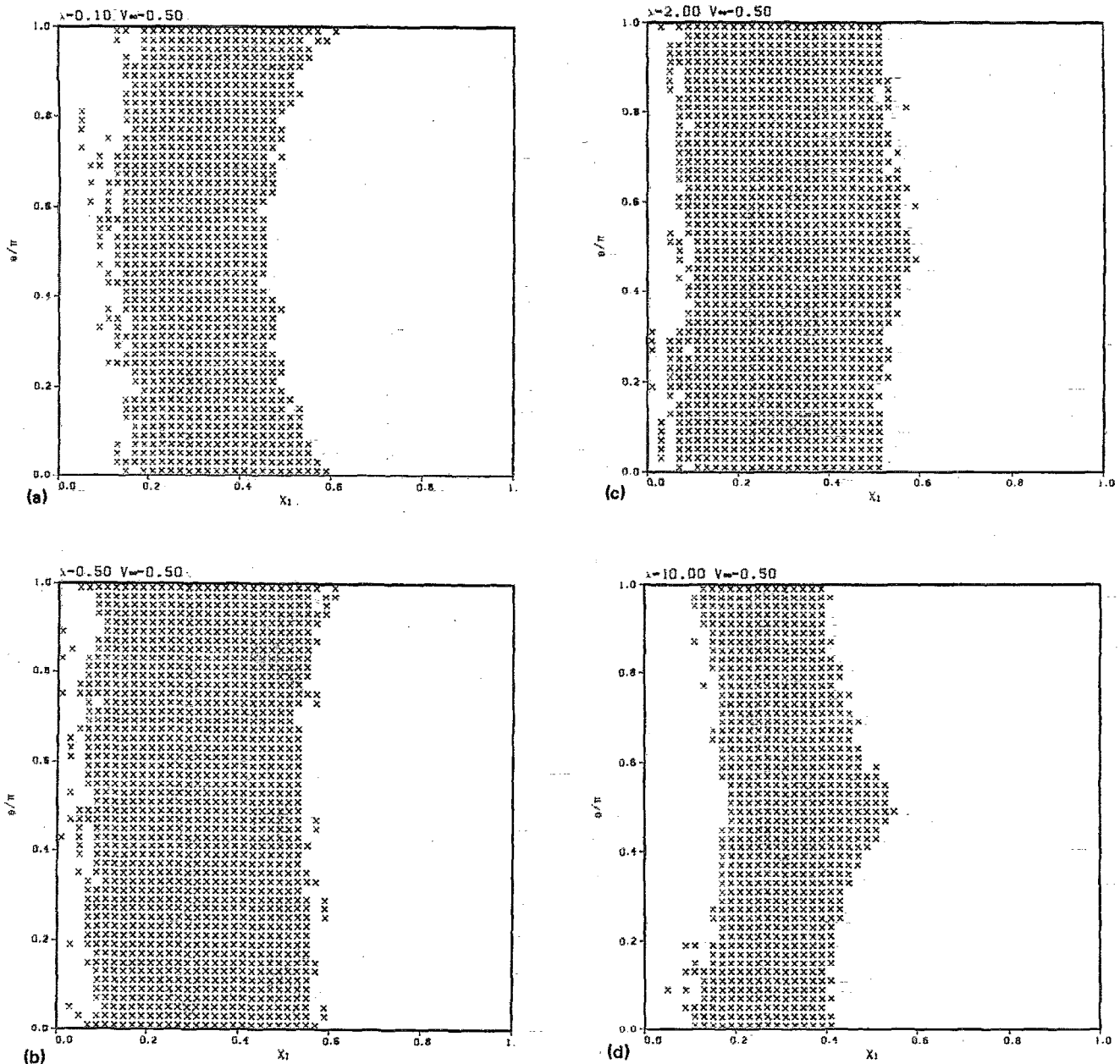


FIG. 7. Plots of the initial values of X_1, θ for spheroidal particles released at $X_2=0.5$ and which are still retained within the initial cell at $t=50$. Points released on a uniform 50×50 grid: (a) $\lambda = 0.1$, $V_\infty = 0.5$; (b) $\lambda = 0.5$, $V_\infty = 0.5$; (c) $\lambda = 2.0$, $V_\infty = 0.5$; (d) $\lambda = 10.0$, $V_\infty = 0.5$. All spherical particles released in the interval $0 < X_1 < 0.603$, for $V_\infty = 0.5$, will be retained.

50%, respectively, of the particles so introduced remained suspended, compared to 60% for spherical particles. Significantly, particles introduced close to the cell boundary at $x_1=0$ are not retained. At larger aspect ratios the extent of particle suspension is reduced with a stronger dependence on orientation. Again at $V_\infty = 0.5$, 37% of the particles remain suspended for $\lambda = 0.1$, 31% for $\lambda = 10$. The plots do not show a clear boundary between the regions where particles are suspended or not, rather it is irregular, especially near $x_1=0$.

Based on these results we conclude that the long-term suspension of spheroidal particles is still possible, at least for times up to $t=50$ or so. We cannot at this point exclude

the possibility that there is some very slow leakage of particles out of the region of particle suspension, which might lead over the extreme long term to all the particles settling out. But we consider this unlikely. The extent of particle suspension is reduced for particles of spheroidal shape, and the reduction is greater with increasing departures from a spherical shape.

IV. SETTLING PARTICLES

We now consider the trajectories of settling particles that are not trapped in the initial cell but cross from one cell to the next in the vertical direction. In doing so we

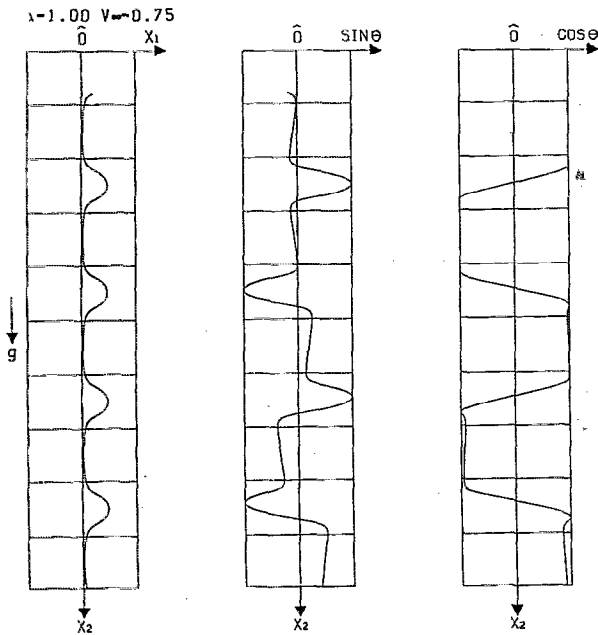


FIG. 8. Sample particle trajectory, path in (X_1, X_2) plane and orientation, of a settling spherical particle: $\lambda = 1.0$; $V_\infty = 0.75$. Initial position $(X_1, X_2) = (0.1875, 0.8125)$. Cells marked at unit intervals.

include information about particle orientation as well as particle position. In Fig. 8 the path and orientation of a spherical particle are shown, where the particle started outside of the suspension region in the initial cell. The path of the particle is regular and periodic, repeating as expected from (26) with period 2 in the vertical direction. The sphere settles rapidly through the cell $1 < x_2 < 2$, where it is swept by the downflow and is then deflected by the upflow in the next cell. This pattern is then repeated. The orientation of the sphere, however, does not have this simple periodic structure, but exhibits a quasiperiodic motion.

It is appropriate at this stage to examine the equation [(25c)] governing the orientation of the particle. For a sphere, $D=0$ and the particle turns only in response to the local vorticity,

$$\frac{d\theta}{dt} = \pi \sin \pi X_1 \sin \pi X_2. \quad (32)$$

In the absence of gravitational settling this rate of rotation is proportional to the particle streamfunction ϕ , (26), which is a constant of motion for a sphere. Under these conditions the local fluid vorticity is constant along a closed particle path and the sphere rotates simply with constant angular velocity. In the presence of gravitational settling, however, the local vorticity is continually changing as a function of particle position. As the path is periodic, so too is the local vorticity. The sphere now rotates (32) but with an angular velocity that itself is a periodic function of time. This leads to the quasiperiodic orientation shown in Fig. 8.

For a spheroid the changing particle orientation is coupled with the velocity of the particle (25) through the difference in the two fall speeds W_1 and W_2 . This leads to

an irregular, aperiodic motion evident in both the particle orientation and the particle path. In Fig. 9 sample trajectories of nonspherical particles are shown. For moderate aspect ratios, $\lambda = 2$ or 0.5 , the particle paths are not too different from the corresponding path of a sphere. The particles shown settle rapidly when close to the cell boundary, in the downflow regions, and are deflected by the upflow regions in alternate cells. Close to $x_1=0$ the fluid vorticity is negligible yet the rate of strain E is large (22). As the particle falls close to this cell boundary it turns to align with the principal axes of the rate of strain, as described earlier, and this is evident in the values of $\sin \theta$ and $\cos \theta$, which take nearly constant values in these intervals. At larger aspect ratios both the particle paths and orientations show strong irregular behavior, indicating that the motion is chaotic.

Finally, we present results (Fig. 10) for the average settling velocity of the particles as the terminal fall speeds for still fluid are varied. These were obtained in the same manner as those for Fig. 6. At $t=0$, 500 particles were released with random initial positions and orientations and their motion followed up until $t=50$. For each particle the settling velocity was zero if it remained trapped, and $2/T_s$ if it settled out where T_s was the time taken to fall between $x_2=2$ and $x_2=4$. An average was then obtained over all the particles released. For a spherical particle the average $\langle V_2 \rangle$ is equal to V_∞ , indicating that the flow has no net effect on the average settling velocity in agreement with earlier results.^{2,3} The nonspherical particles settle on average more rapidly. This in part may be attributed to the reduction in the number of particles held in suspension.

V. CHAOTIC MOTION

The observation of irregular motion in the trajectories of nonspherical particles raises the question of whether or not the particle motion is chaotic. Chaotic motion of Lagrangian fluid elements in various unsteady two-dimensional flows is a well-known phenomena²⁰⁻²² and has been found to occur in the three-dimensional steady ABC flow.²³ It has been observed even in unsteady cellular flow fields by Smith and Spiegel.²⁴ Here the flow field is steady and two dimensional, and the motion of both Lagrangian fluid elements and spherical particles is completely regular. Any chaotic behavior must be a result of the tumbling motion of the spheroidal particles.

As an initial investigation of this question some Poincaré sections were obtained. Plots of the $(X_1, 0)$ coordinates were made for successive intersections of a particle trajectory with the level $X_2=2n + 1/2$ for arbitrary integers n , explicitly using the periodicity of the flow. By this means we can obtain sections for both suspended and settling particles. Figure 11(a) shows the section for the regular motion of a suspended spherical particle, corresponding to the trajectory shown previously in Fig. 5. The path repeatedly intersects the midlevel $X_2 = 1/2$ at the same two values of X_1 . But for the reasons noted in the previous section the period of the sphere orientation is in general not rationally related to the period of the path in (x_1, x_2) plane. This leads to the continuous line of values for θ , between 0

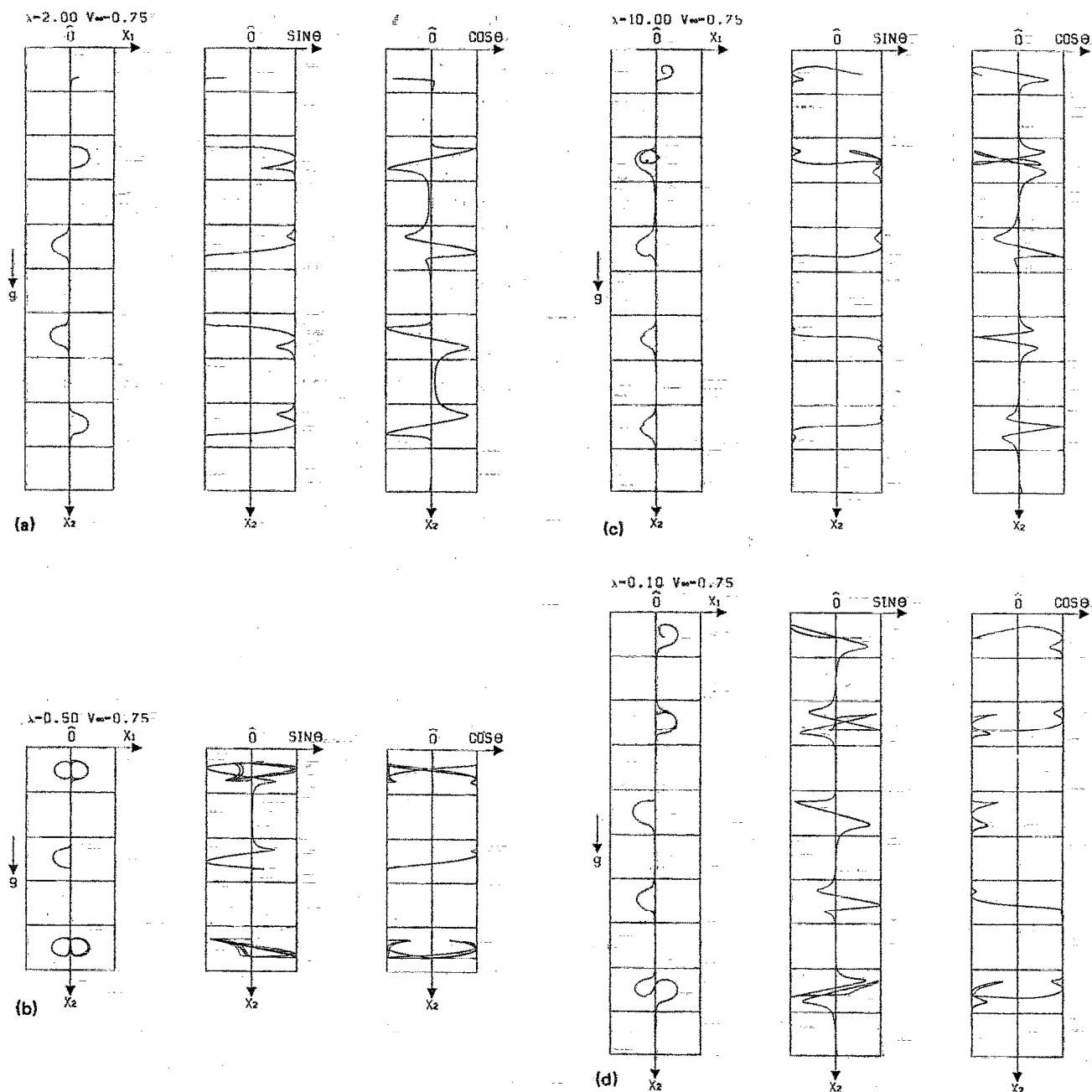


FIG. 9. Sample trajectories of settling spheroidal particles, path and orientation for $V_{\infty} = 0.75$, cells marked at unit intervals: (a) $\lambda = 2$, initial point $(X_1, X_2) = (0.1875, 0.6875)$; (b) $\lambda = 0.5$, initial point as in (a); (c) $\lambda = 10.0$, initial point $(0.1875, 0.5625)$; (d) $\lambda = 0.1$, initial point as in (c).

and π , at the intersection with $X_2 = \frac{1}{2}$. The other sections [Figs. 11(b) and 11(c)] for suspended nonspherical particles have the same general features of regular motion. There are two distinct values of X_1 at the intersection, which are modified by the corresponding particle orientation and hence settling velocity at these points.

The Poincaré sections of Figs. 11(d)–11(f) are for settling particles and correspond to trajectories whose initial stages were previously given in Figs. 8 and 9. The path of a spherical particle is regular in the (x_1, x_2) plane repeating with period 2 in the x_2 direction. There is a single value of X_1 corresponding to the intersection with $X_2 = \frac{1}{2} \pmod{2}$, which is apparent in Fig. 11(d). Again there is a continu-

ous range of values of θ at the intersection due to the noncommensurate periods for motion in the x_2 direction and particle rotation. By comparison, there is considerable scatter in the sections for the nonspherical settling particles, indicating at least weakly chaotic motion.

Finally, we present in Fig. 12 power spectra for the time series of the particle orientation m_1 , equal to $\cos \theta$, to indicate whether the motion is quasiperiodic or aperiodic. The settling sphere of Fig. 12(a) shows strong periodicity with several harmonics. The suspended spheroid of Fig. 12(b) exhibits less structure, but the spectrum has distinguishable frequencies and harmonics, while the settling spheroid of Fig. 12(c) gives rise to a continuous, broad-

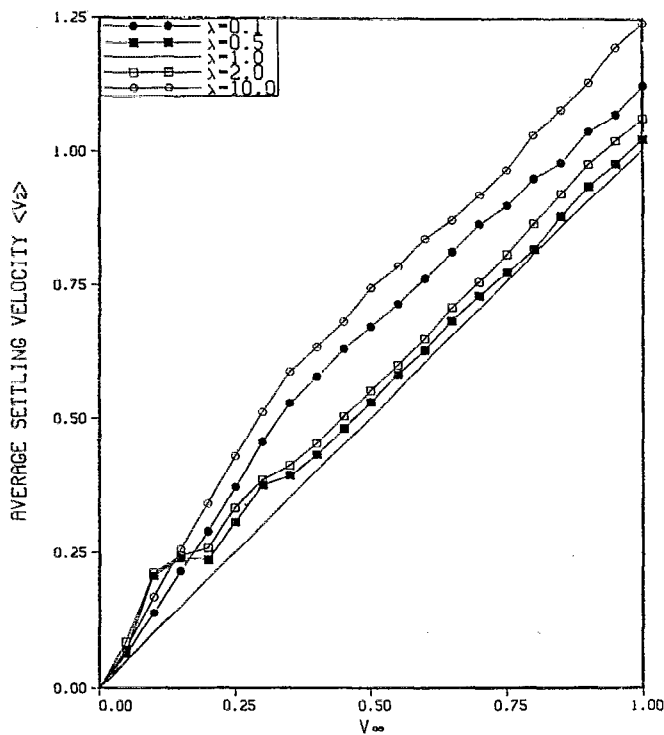


FIG. 10. Average vertical settling velocity $\langle V_2 \rangle$ of spheroidal particles for various aspect ratios λ , against the spherically averaged fall speed V_∞ .

band spectrum. The dynamical coupling of particle orientation to particle velocity ensures that these spectra are also representative of the velocities of nonspherical particles. Other spectra not shown here have similar features and Fig. 12 is typical for the particle motion. The spectra were produced by the IMSL routine FTFPS,¹⁹ based on a record of 20 480 data points.

Based on the results so far we conclude that suspended spheroidal particles have a regular, quasiperiodic motion but that settling spheroidal particles have a chaotic tumbling motion. The extent of the chaotic motion and its specific dependence on the parameters, such as aspect ratio λ , will require further investigation. We note that the system of equations (25) governing the particle motion, restricted to planar orientation, is a third-order autonomous system. This is the lowest order for an unforced dynamical system to exhibit chaotic motion.²⁵ By contrast, the system studied by Jeffery⁹ for steady, uniform shear resulted in only a second-order system since m_3 could be determined from m_1 and m_2 and gave rise to regular periodic motion. Thus the combination of nonuniform velocity gradients and particle tumbling are required for chaotic motion. We note also that we would not expect an attractor in this system since it is not dissipative, nor is the divergence in phase space $-(X_1, X_2, \theta)$ strictly negative. The divergence is given by

$$\begin{aligned} \frac{\partial}{\partial X_1} (\dot{X}_1) + \frac{\partial}{\partial X_2} (\dot{X}_2) + \frac{\partial}{\partial \theta} (\dot{\theta}) \\ = -2D\pi \cos \pi X_1 \cos \pi X_2 \cos 2\theta, \end{aligned} \quad (33)$$

which changes sign frequently during the course of the motion.

VI. PARTICLES WITH INERTIA

A full discussion of the modifying effects of particle inertia on the results presented so far is beyond the scope of this paper. But in this initial investigation we did make some limited calculations to see what might be expected to arise and whether or not the chaotic motion would persist. Previous experience with spherical particles² has shown that weak inertial effects over a long period of time lead to very organized regular particle trajectories, and the possibility exists that particle inertia would reduce or eliminate the chaotic tumbling of the spheroidal particles. The equations of motion when particle inertia is included are more complex than those treated up until now, Eqs. (10)–(12). The full equations of motion are summarized in the Appendix.

Besides the parameters V_∞ for the settling velocity and λ for the aspect ratio, an additional parameter must be specified for the inertial response time of the particle. This is defined here as a spherically averaged value $1/\alpha$ by Eq. (A4). This time scale together with the other two parameters are sufficient to completely specify the particle motion of a spheroidal particle. The nondimensional value of α is given in terms of the scales L, U_0 of the cellular flow field as $A = \alpha L / U_0$.

At a settling velocity $V_\infty = 0.5$, a spherical particle subject to weak inertia, $A = 10$, eventually follows a well-defined asymptotic trajectory that is insensitive to the initial particle position. All particles settle and there is no long-term particle suspension. For $A = 1.0$ the motion is no longer organized and shows no structure, except again for the absence of particle suspension, while for $A = 0.1$ the motion is again structured in the long term with the particles settling vertically along the vertical cell boundaries, apparently with little direct influence from the flow. At the same settling velocity, a nonspherical oblate spheroid with aspect ratio $\lambda = 0.1$ shows similar characteristics. For weak particle inertia, $A = 10$, there is no obvious chaotic motion by $t = 200$ and the particles appear to collect into regular asymptotic paths as did the spherical particles. For $A = 1.0$ the motion is chaotic and disorganized, while for $A = 0.1$ the particles eventually settle along nearly vertical paths close to the cell boundaries but somewhat displaced from them.

These results are only suggestive of how particle inertia may modify the particle motion and further work on this topic is needed. The general indications are that weak inertia or very strong inertia over a long period of time will indeed reduce or eliminate the chaotic motion.

VII. CONCLUSION

In this paper we have addressed the question of whether or not nonspherical particles may be suspended by a simple, steady cellular flow and some of the general characteristics of the particle motion. The results indicate that suspension still occurs but is reduced as departures from

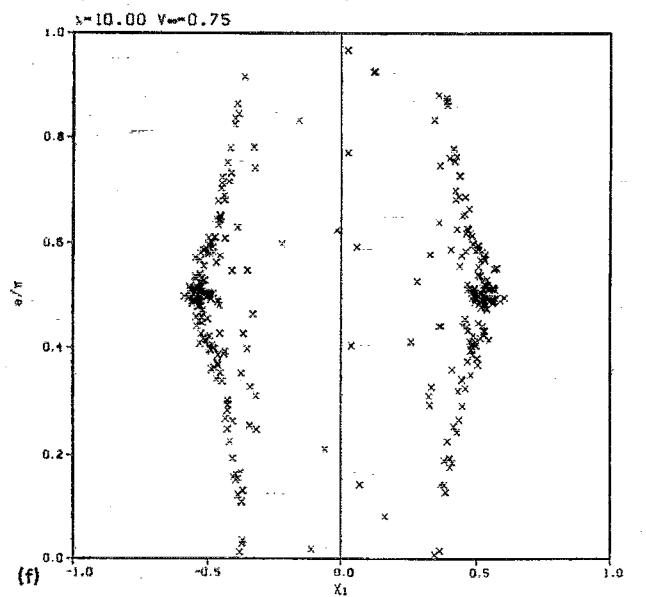
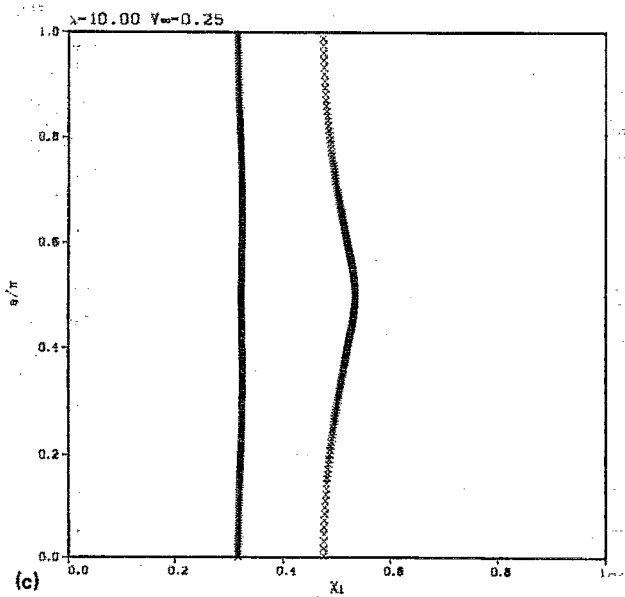
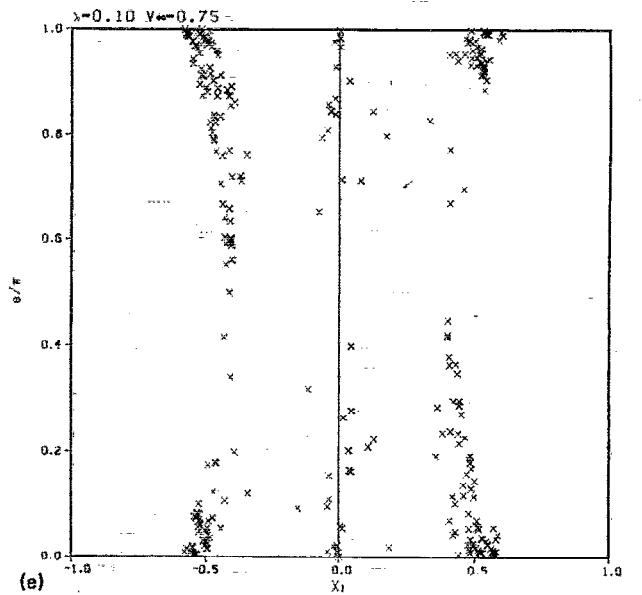
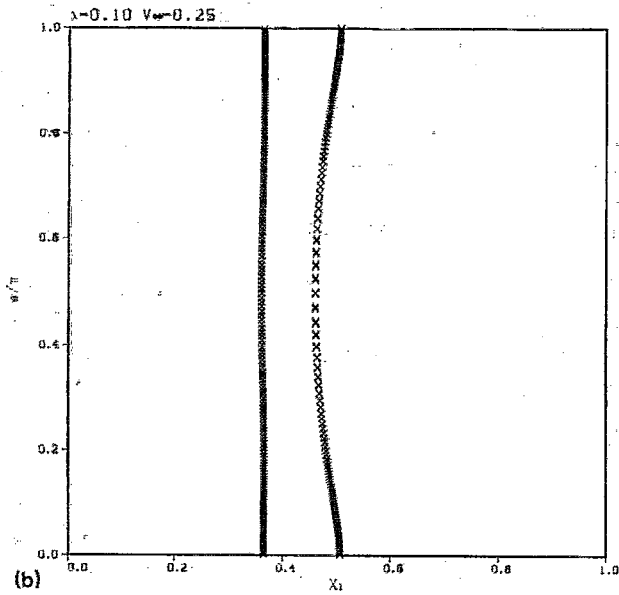
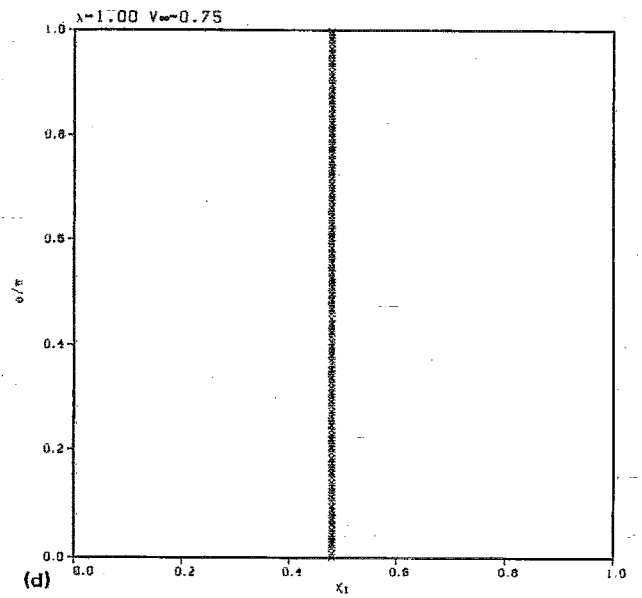
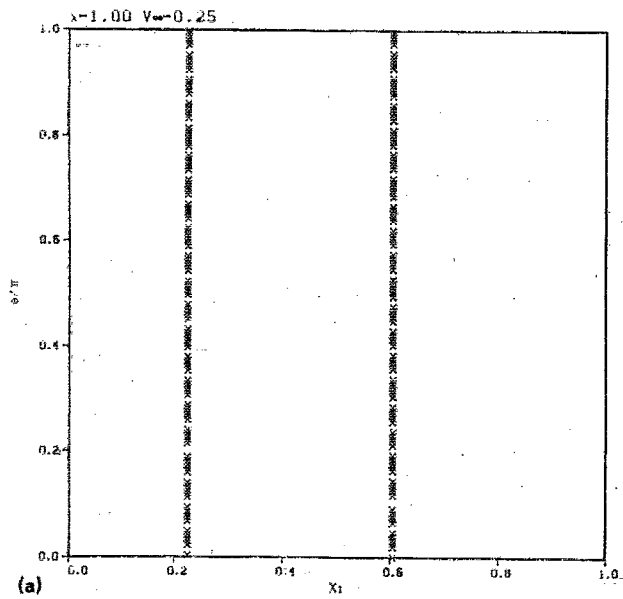


FIG. 11. Poincaré sections of particle trajectories showing values of (X_1, θ) at the intersections of the trajectory with $X_2 = 2n + 1/2$, for integers n . Suspended particles, initial positions as in Fig. 5: (a) $\lambda = 1$ (sphere), $V_\infty = 0.25$; (b) $\lambda = 0.1$, $V_\infty = 0.25$; (c) $\lambda = 10.0$, $V_\infty = 0.25$. Settling particles, initial positions as in Figs. 8 and 9: (d) $\lambda = 1$ (sphere), $V_\infty = 0.75$; (e) $\lambda = 0.1$, $V_\infty = 0.75$; (f) $\lambda = 10.0$, $V_\infty = 0.75$.

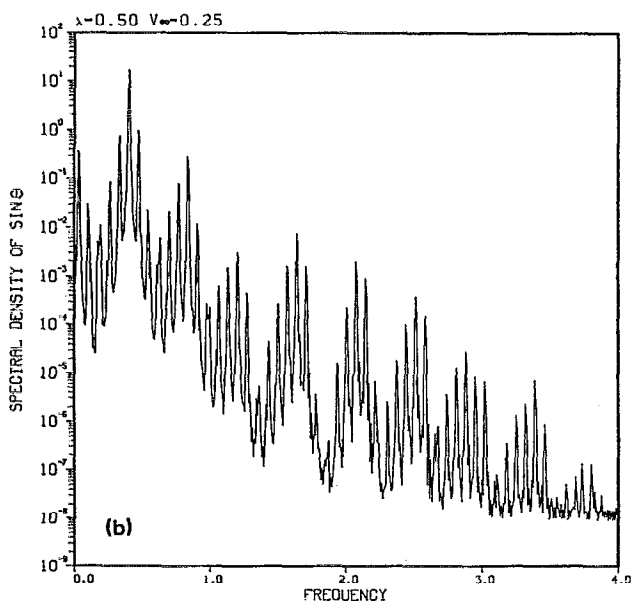
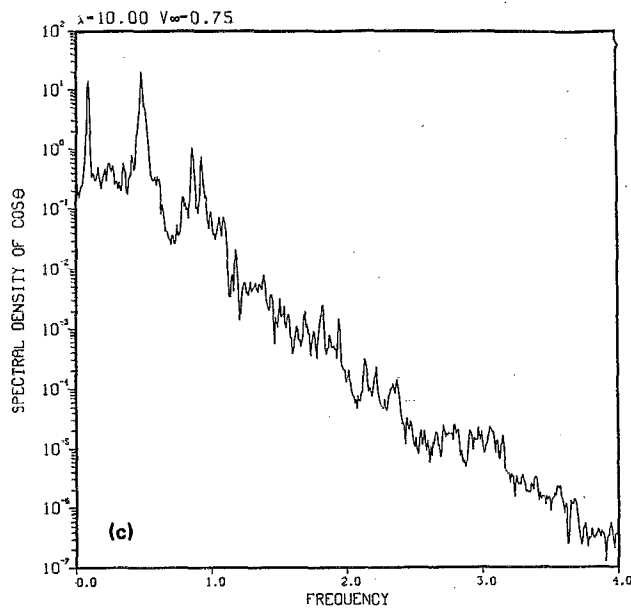
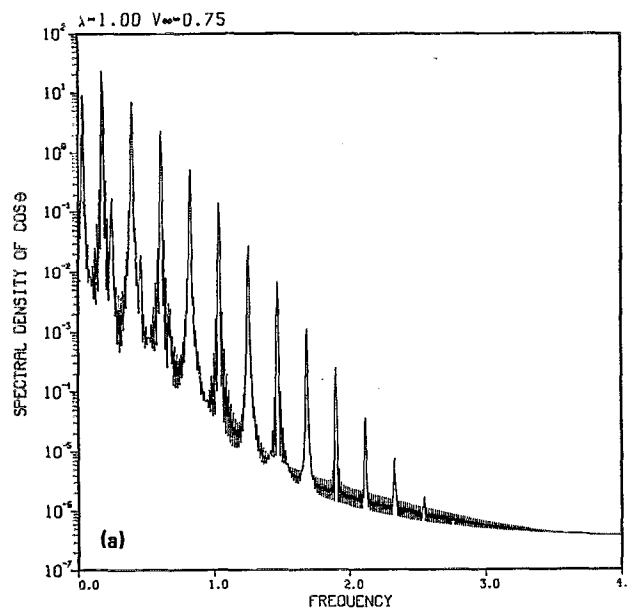


FIG. 12. Power spectra of the time series for particle orientation along a trajectory; (a) spherical particle, $\lambda = 1$, $V_\infty = 0.75$, (see Fig. 8); (b) spheroidal suspended particle, $\lambda = 0.5$, $V_\infty = 0.25$ [see Fig. 5(b)]; (c) settling spheroidal particle, $\lambda = 10$, $V_\infty = 0.75$ [see Fig. 9(c)].

spherical shape increase. In the process we have found that the motion of these nonspherical particles is in many cases chaotic. This raises many issues that will require further study and we have presented here only a preliminary investigation of the chaotic behavior. Recent work by Shin²⁶ has confirmed our speculation that particle suspension still occurs, and this will be reported on in the near future. Of practical significance is that chaotic mixing of nonspherical particles may occur in laminar flows, analogous to the processes in Lagrangian turbulence.²² Second, based on the general features of our results we may expect chaotic orientations of nonspherical particles to be possible in other flows that have either nonuniform or unsteady velocity gradients.

ACKNOWLEDGMENT

The work reported in this paper was carried out with support from the DARPA-URI Program under Contract No. ONR-N00014-86-K0754.

APPENDIX: PARTICLES WITH INERTIA

In this appendix we specify the equations of motion appropriate to a spheroidal particle subject to the effects of particle inertia. The momentum equation for a particle of mass m_p is

$$m_p \frac{d\mathbf{V}}{dt} = \mathbf{F} + m_p \mathbf{g}, \quad (\text{A1})$$

where the fluid force on the particle \mathbf{F} is specified by (5). Referred to the symmetry axes of the particle and the unit vector \mathbf{m} along the axis of symmetry,

$$K_{ij} = K_1 m_i m_j + K_2 (\delta_{ij} - m_i m_j). \quad (\text{A2})$$

Thus

$$m_p \frac{d\mathbf{V}}{dt} = \mu K_1 \mathbf{m} \mathbf{m} \cdot (\mathbf{u} - \mathbf{V}) + \mu K_2 [(\mathbf{u} - \mathbf{V}) - \mathbf{m}(\mathbf{u} - \mathbf{V}) \cdot \mathbf{m}] + m_p \mathbf{g}, \quad (\text{A3})$$

where \mathbf{u} denotes the local fluid velocity $\mathbf{u}(\mathbf{X}(t), t)$. The inertial response time for motion parallel to \mathbf{m} is $m_p/\mu K_1$ and $m_p/\mu K_2$ for motion normal to the axis of symmetry. It is convenient to define a spherically averaged inertial response time $1/\alpha$ by

$$\frac{1}{\alpha} = \frac{m_p}{3\mu} \left(\frac{1}{K_1} + \frac{2}{K_2} \right), \quad (\text{A4})$$

similar to the definition (17) for V_∞ . In terms of α and V_∞ the equation of motion is

$$\frac{1}{\alpha} \frac{d\mathbf{V}}{dt} = \frac{1}{3} (2 + \Lambda^{-1}) [(\Lambda - 1)(\mathbf{u} - \mathbf{V}) \cdot \mathbf{m} \mathbf{m} + (\mathbf{u} - \mathbf{V})] + V_\infty \hat{\mathbf{g}}, \quad (\text{A5})$$

the ratio $\Lambda = K_1/K_2$ is given by (14) and (15).

Explicit values of K_1, K_2 for prolate spheroids, $\lambda > 1$ and $\tau^2 = \lambda^2 - 1$, are¹⁶

$$K_1 = 8\pi b \tau^3 [(2\tau^2 + 1)\log(\lambda + \tau) - \lambda\tau]^{-1}, \quad (\text{A6})$$

$$K_2 = 16\pi b \tau^3 [(2\tau^2 - 1)\log(\lambda + \tau) + \lambda\tau]^{-1}, \quad (\text{A7})$$

and for an oblate spheroid, $\lambda < 1$ and $\tau^2 = 1 - \lambda^2$,

$$K_1 = 8\pi b \tau^3 [(2\tau^2 - 1)\tan^{-1}(\tau/\lambda) + \lambda\tau]^{-1}, \quad (\text{A8})$$

$$K_2 = 16\pi b \tau^3 [(2\tau^2 - 1)\tan^{-1}(\tau/\lambda) - \lambda\tau]^{-1}. \quad (\text{A9})$$

From these results the inertial response time parameter $1/\alpha$ can be evaluated.

The angular momentum for rotation about the center of mass of the particle is given by $I_{ij}\Omega_j$ where \mathbf{I} is the moment of inertia tensor, which for a spheroidal particle is

$$I_{ij} = I_1 m_i m_j + I_2 (\delta_{ij} - m_i m_j). \quad (\text{A10})$$

The principal moments I_1 and I_2 are $\frac{2}{3}m_p b^2$ and $\frac{1}{3}m_p (a^2 + b^2)$, respectively. The rate of change of angular momentum is equal to the resultant fluid torque \mathbf{G} , determined by b , and

$$\frac{d}{dt} (I_{ij}\Omega_j) = G_i. \quad (\text{A11})$$

However, the specification of I_{ij} of (A10) involves the body-symmetry axis \mathbf{m} , which rotates with the body, so that (A11) takes the form of the Euler equations for rigid body motion²⁷ in a rotating frame. Here, these can be written as

$$I_2 \dot{\Omega} + (I_1 - I_2)(\dot{\Omega} \cdot \mathbf{m})\mathbf{m} - (I_2 - I_1)(\Omega \cdot \mathbf{m})\Omega \times \mathbf{m} = \mathbf{G}, \quad (\text{A12})$$

In line with our earlier discussion the fluid torque \mathbf{G} acting on a spheroidal particle is

$$\begin{aligned} \mathbf{G} = & \mu \{ R_1 (\frac{1}{2} \boldsymbol{\omega} - \boldsymbol{\Omega}) \cdot \mathbf{m} \mathbf{m} \\ & + R_2 [(\frac{1}{2} \boldsymbol{\omega} - \boldsymbol{\Omega}) - (\frac{1}{2} \boldsymbol{\omega} - \boldsymbol{\Omega}) \cdot \mathbf{m} \mathbf{m}] \} \\ & + \mu R_2 D \mathbf{m} \times (\mathbf{E} \cdot \mathbf{m}). \end{aligned} \quad (\text{A13})$$

The local fluid vorticity $\boldsymbol{\omega}$ is evaluated at the center of the particle $\mathbf{X}(t)$ as is the local rate of strain \mathbf{E} . The coefficient D is given by (16). Explicit values of R_1 and R_2 for prolate spheroids, $\lambda > 1$ and $\tau^2 = \lambda^2 - 1$, are¹⁶

$$R_1 = \frac{16}{3} \pi b^3 \tau^3 [\lambda\tau - \log(\lambda + \tau)]^{-1}, \quad (\text{A14})$$

$$R_2 = \frac{16}{3} \pi b^3 \tau^3 (1 + \lambda^2) [(2\tau^2 + 1)\log(\lambda + \tau) - \lambda\tau]^{-1}, \quad (\text{A15})$$

and for an oblate spheroid, $\lambda < 1$ and $\tau^2 = 1 - \lambda^2$,

$$R_1 = \frac{16}{3} \pi b^3 \tau^3 [\tan^{-1}(\tau/\lambda) - \lambda\tau]^{-1}, \quad (\text{A16})$$

$$R_2 = \frac{16}{3} \pi b^3 \tau^3 (1 + \lambda^2) [\lambda\tau + (2\tau^2 - 1)\tan^{-1}(\tau/\lambda)]^{-1}. \quad (\text{A17})$$

From (A12) and the above specification of the fluid torque the rate of change of the angular velocity $\boldsymbol{\Omega}$ can be determined.

¹H. Stommel, *J. Mar. Res.* 8, 24 (1949).

²M. R. Maxey and S. Corrsin, *J. Atmos. Sci.* 43, 1112 (1986).

³M. R. Maxey, *Phys. Fluids* 30, 1915 (1987).

⁴H. R. Fruppacher and J. D. Klett, *Microphysics of Clouds and Precipitation* (Reidel, Dordrecht, The Netherlands, 1978), pp. 328-346.

⁵B. D. Marsh and M. R. Maxey, *J. Volcanol. Geotherm. Res.* 24, 95 (1985).

⁶H. K. Moffatt, *Rep. Prog. Phys.* 46, 621 (1983).

⁷S. R. Dungan and H. Brenner, *Phys. Rev. A* 38, 3601 (1988).

⁸M. R. Maxey, *J. Fluid Mech.* 174, 441 (1987).

⁹G. B. Jeffery, *Proc. R. Soc. London Ser. A* 102, 161 (1922).

¹⁰H. Brenner, *J. Colloid Interface Sci.* 71, 189 (1979).

¹¹H. Brenner, *J. Colloid Interface Sci.* 80, 548 (1981).

¹²L. H. Dill and H. Brenner, *J. Colloid Interface Sci.* 94, 430 (1983).

¹³H. Cho, J. V. Iribane, and W. G. Richard, *J. Atmos. Sci.* 38, 1111 (1981).

¹⁴H. Kagermann and W. E. Koehler, *Physica A* 116, 178 (1982).

¹⁵E. M. Krushkal and I. Gallily, *J. Colloid Interface Sci.* 99, 141 (1984).

¹⁶J. Happel and H. Brenner, *Low Reynolds Number Hydrodynamics* (Prentice-Hall, Englewood Cliffs, NJ, 1965).

¹⁷R. Clift, J. R. Grace, and M. E. Weber, *Bubbles, Drops and Particles* (Academic, New York, 1978).

¹⁸F. P. Bretherton, *J. Fluid Mech.* 14, 284 (1962).

¹⁹J. R. Rice, *Numerical Methods, Software and Analysis* (McGraw-Hill, New York, 1983).

²⁰H. Aref, *J. Fluid Mech.* 143, 1 (1984).

²¹J. Chaiken, C. K. Chu, M. Tabor, and Q. M. Tan, *Phys. Fluids* 30, 687 (1987).

²²J. M. Ottino, *Annu. Rev. Fluid Mech.* 22, 207 (1990).

²³T. Dombre, U. Frisch, J. M. Greene, M. Heron, A. Mehr, and A. M. Soward, *J. Fluid Mech.* 167, 353 (1986).

²⁴L. A. Smith and E. A. Spiegel, *Lect. Notes Phys.* 230, 306 (1985).

²⁵J. Guckenheimer and P. Holmes, *Nonlinear Oscillations, Dynamical Systems and Bifurcations of Vector Fields* (Springer-Verlag, New York, 1983).

²⁶H. Shin, Ph.D. thesis dissertation, Brown University, 1990.

²⁷H. Goldstein, *Classical Mechanics* (Addison-Wesley, Reading, MA, 1950).